Supplementary Information (SI) for New Journal of Chemistry.

Hardwood-Derived Lignin as a Tribo-Positive Filler in Electrospun PVDF Nanofibers for Efficient Triboelectric Energy Harvesting

Deepak Jyoti Deuri[a], Jiwajyoti Mahanta[b], Bipasha Saikia [c], Bikash Kumar Das[c], Brajendra K. Sharma[d], Jaemin Kim[e], Parikshit Gogoi[a*]

[a]Department of Chemistry, Nowgong College (Autonomous), Nagaon 782011, Assam, India

[b]Department of Chemical Engineering, Indian Institute of Technology Guwahati, India

[c]Department of Chemistry Department, Indian Institute of Technology Guwahati, India

[d]US Department of Agriculture, Agricultural Research Service Eastern Regional Research Center, Sustainable Biofuels and Coproducts Research, Wyndmoor, PA 19038-8598, USA

[e]Illinois Sustainable Technology Center, University of Illinois at Urbana-Champaign, Champaign, IL 61820, USA

*Corresponding author. E-mail address: parikk100@gmail.com

Electronic Supporting Informations

Table S1. A assignment of peaks in Fourier transform infrared (FTIR) analysis and their correlation to functional groups in lignin.

Frequency (cm^{-1})	Assignments
1030	C–O(H) + C–O(C) (first order aliphatic OH and ether
1270	C–O stretching vibration of secondary alcohol
1462	Lignin (C-H bending in CH_2 and CH_3)
1513	C–C stretching (aromatic skeleton
1590	Aromatic skeletal vibration
1660	Lignin (C=O stretching)

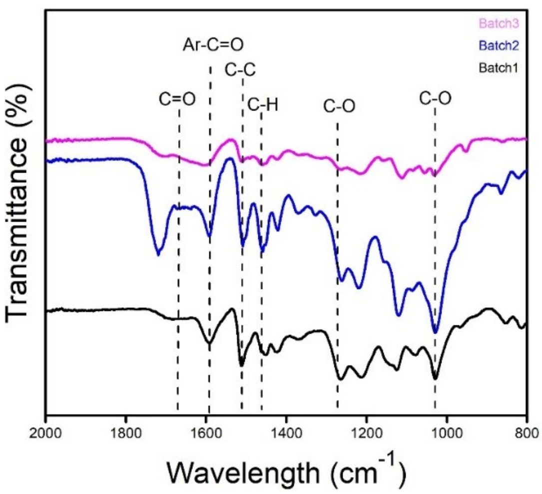

Fig S1. FTIR Spectrum of alkali lignin of multiple batches.

Table. S2. Yields of obtained lignin.

Biomass feedstock loading	Chemical composition			Solid recovery %	Lignin removal %	Lignin yield %
	Cellulose%	Hemicellulose%	Lignin %			
Raw Biomass (Tectona Grandis)	34	29.7	17.5	-	-	-
Batch 1	67.3	14.4	4.8	50.6	85.2	13.88
Batch 2	63.6	13.6	6.8	50.4	85.2	19.58
Bacth 3	58.4	17.4	5.9	55	80	18.54

The chemical composition of prior to and following pretreatment was assessed using the NREL analytical technique.[1] The contents of cellulose and hemicellulose were determined based on the total quantities of their component monomers. The relevant calculation equations are stated as follows.

$$\text{Lignin yield (\%)} = \mathit{Solids\ recovery}\ (\%) \times \frac{\mathit{Lignin\ content\ in\ pretreated\ solids}\ (\%)}{\mathit{Lignin\ content\ in\ raw\ biomass}\ (\%)}$$

$$\text{Lignin removal (\%)} = \left(1 - \frac{\mathit{Mpretreated} \times \mathit{Plignin}}{\mathit{Mlignin\ of\ raw\ biomass}}\right) \times 100$$

Table S3. NMR assignments of major interlinks in 2D-HSQC NMR spectra of lignin.

Label	$\delta c/\delta_H$ (ppm)	Assignments
B_β	53.7/3.37	C_β-B_β in phenylcoumaran
C_β	54.2/3.06	C_β-B_β in B_β- $B_{\beta'}$ resinol
$-OCH_3$	56.0/3.74	C-H in methoxyls
A_γ	60.9/3.38	C_γ-H_γ in $_\gamma$-hydroxylated β-O-4’
B_γ	62.4/3.63	C_γ-H_γ in phenylcoumaran
A'_γ	64.7/3.94	C_γ-H_γ $_\gamma$-acetylated β-O-4’
C_γ	70.1/3.94	C_γ-H_γ in β- β’ resinol
Aα	72.35/4.85	Cα-Hα in β-O-4 substructures (A)
A_β(H)	81.3/4.61	C_β-B_β in β-O-4’ linked to a H-unit
A_β(G)	84.3/4.29	C_β-B_β in β-O-4’ linked to a G-unit
Cα	85.7/4.62	Cα-Hα in β-β’ resinol
A_β(H)	81.3/4.61	C_β-B_β in β-O-4’ linked to a H-unit
A_β(G)	84.3/4.29	C_β-B_β in β-O-4’ linked to a G-unit
Cα	85.7/4.62	Cα-Hα in β-β’ resinol
A_β(S)	86.0/4.14	C_β-B_β in β-O-4’ linked to a S-unit

$S_{2,6}$	104.4/6.71	C_2-H_2 and C_6H_6 in etherified syringyl units (S)
$S'_{2,6}$	104.7/7.36	C_2-H_2 and C_6H_6 in etherified syringyl units (S’)
G_2	112.0/7.68	C_2-H_2 in guaiacyl units (G)
PCA_β and FA_β	116.7/6.39	C_β-B_β in p-coumarate (PCA)
G_5	115.9/6.69	C_5-H_5 in guaiacyl units (G)
G_6	119.3/6.77	C_6-H_6 in guaiacyl units (G)
$PCA_{3.5}$	115.4/6.68	C_3-H_3 in C_5- H_5 in p-coumarate (PCA)
$H_{2,6}$	128.6/7.04	$C_{2,6}$-$H_{2,6}$ in p-hydroxyphenyl units (H)
$PCA_{2,6}$	130.7/7.49	C_2-B_2 and C_6-H_6 in p-coumarate (PCA)

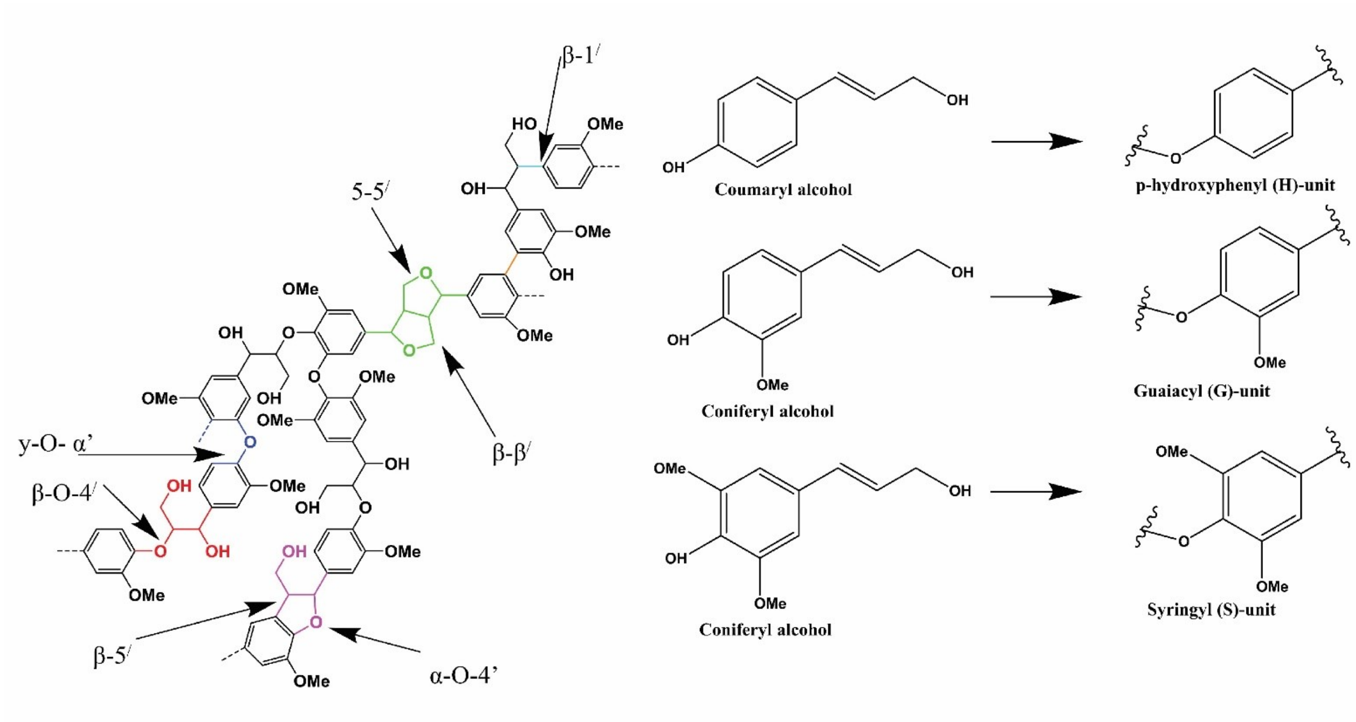

Fig S2**.** Main lignin inter-unit linkage, chemical structures of monolignol, and of the derived units

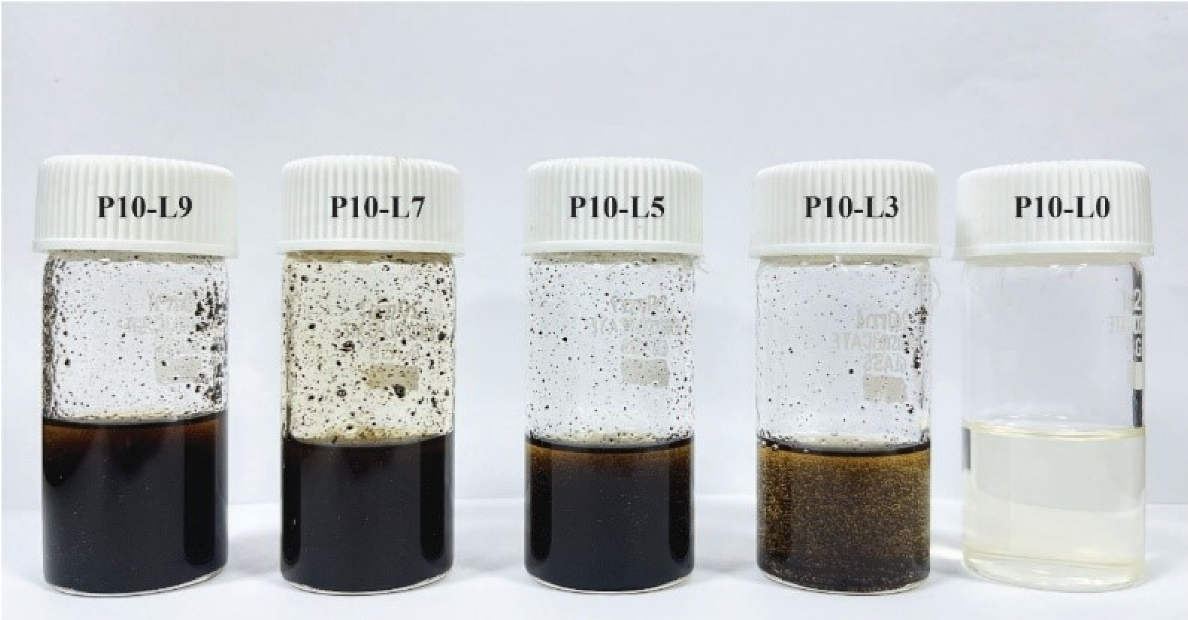

Fig. S3. Digital photographs of the P10-L0 , PL solutions (lignin concentrations are 3 wt% , 5wt%, 7wt%, and 9 wt% , respectively.

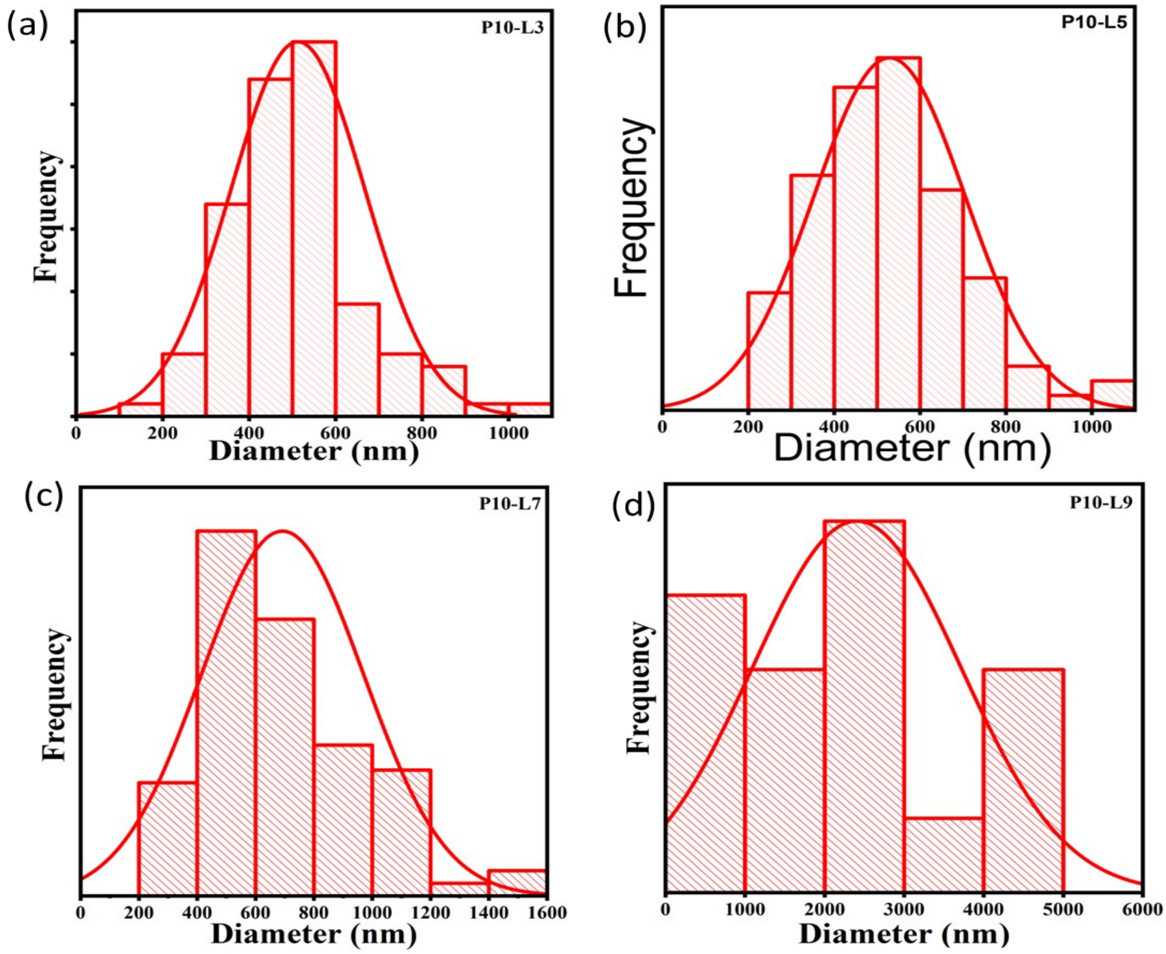

Fig. S4. Histogram depicting the distribution of nanofiber diameters and the curve representing the lognormal distribution of lignin-PVDF with different concentrations

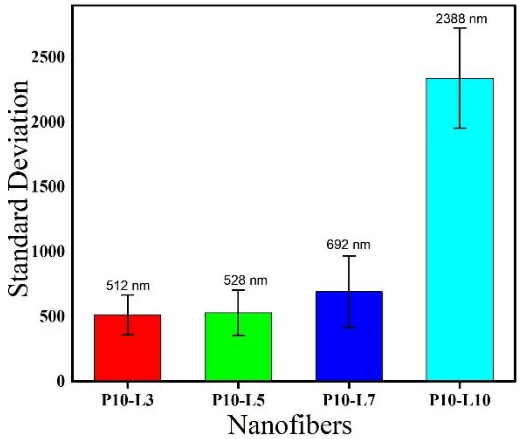

Fig S5. The standard deviation of the diameters of nanofibers in PLNF composites with different lignin content.

Table S4. Lignin-PVDF with various concentrations and observations of nanofiber of different average diameters and standard deviation.

	PVDF (wt%)	Lignin (wt%)	Observations	Average Diameter (nm)	Standard Deviation
P10-L3	10	3	Uniform fibers	488.2	153.9244
P10-L5	10	5	Uniform fibers	505.3	175.4753
P10-L7	10	7	Beads on strings	586.7	276.7745
P10-L9	10	9	Beads on strings	2338.996	386.9155

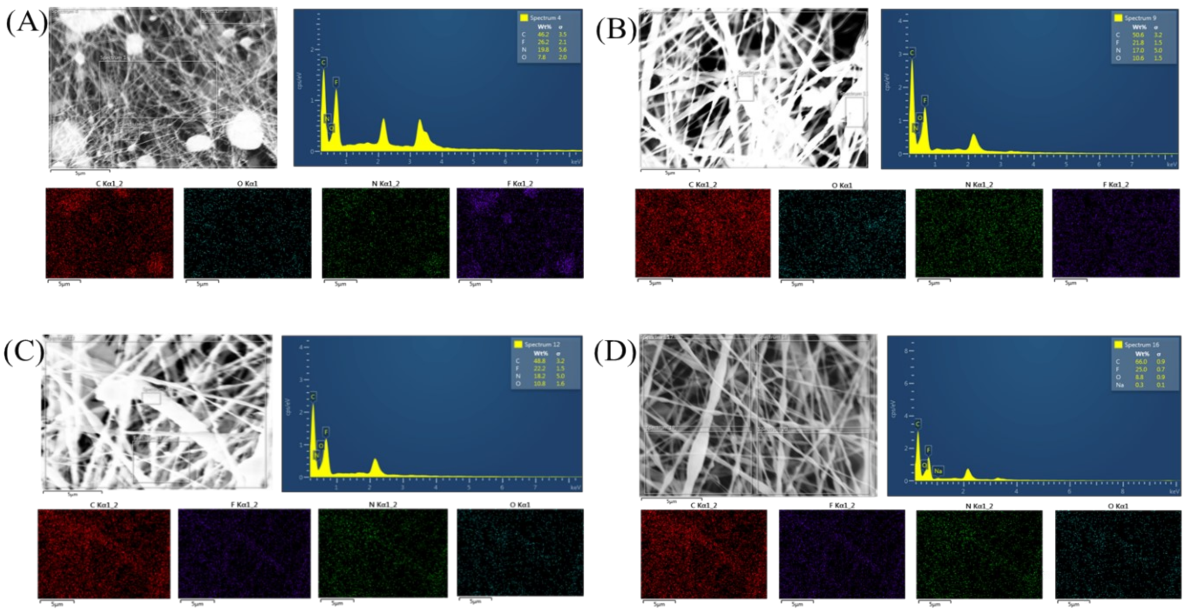

Fig S6. FESEM images along with their corresponding EDS elemental maps. (A) Pure PVDF NF, (B) P10-L5, (C) P10-L7, and (D) P10-L9

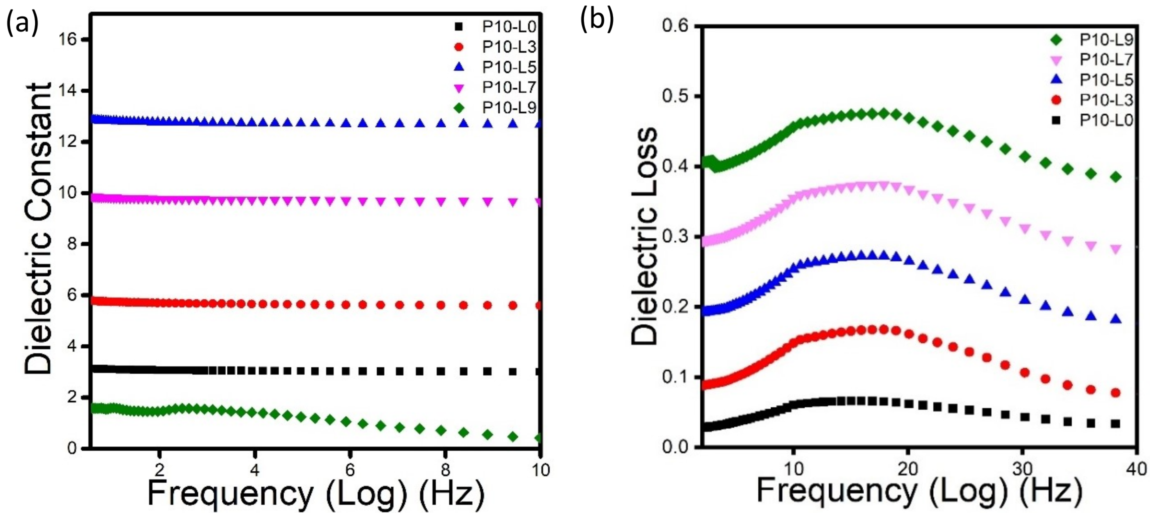

Fig S7. Dielectric Constant and Dielectric Loss of P10-L0, P10-L3, P10-L5, P10-L7, P10-L9 nanofibers

Table S5. The Dielectric Constant and Dielectric Loss of PLNF-TENGs with different compositions.

	Dielectric Constant	Dielectric Loss
P10-L0	3.23	0.01
P10-L3	5.92	0.06
P10-L5	12.97	0.03
P10-L7	9.97	0.06
P10-L9	4.33	0.05

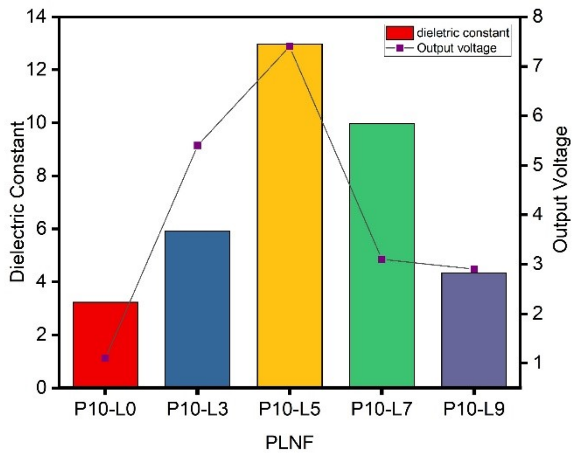

Fig S8. The correlation plot between dielectric constant and output voltage of PLNF composites.

Table S6. The Comparison of the performance of TENGs from various materials, including biomaterials.

Materials	**Fabrication method**	**Contact area**	**Conditions**	**Current**	**Voltage**	**Power Density (mW/m^2)**	**Sustainability**	**References**
TiO_2NP	Electrospinning	10 cm × 10 cm	5–10 Hz	−1.61 µA	111 V	23.44 mW m^{-2}	Biocompatibility, Mechanical durability	[2]
chitosan-diatom	Casting	3 × 4 cm^2	3Hz, 5Hz, 7Hz, 10 Hz	1.02 µA	150 V	15.7 mW/m^2	skin-attachable	[3]
PCA PNFMTPU /CB BNFM	Electrospinning	4x4 cm^2			24.45 V	**6** mW/m^2	Biocompatibility, human motion detection	[4]
PI/TPU-TPU	Electrospinning	-	4Hz/5kPa		0.92 V	-	Fingertip interaction force detection, pronunciation sensing, human motion and finger gesture recognition	[5]
CMCSCM C-Na	Electrospinning	9 cm^2	2Hz	20 nA	3V	120 mWm^{-2}	Water soluble	[6]
CANF	Electrospinning	1.27 cm^2	3 N, 4Hz	0.4 mA/m^2	25 V	16 mW/m^2	Tactile and proximity sensing	[7]
PEI-GO in CS	Casting	3 and 6 cm	1.0–6.0 Hz	6.6 µA	222 V	407 mW/m^2)	fully bioderived	[8]
Lignin/PVDF	Electrospinning	2x2 cm^2	1Hz,3Hz,5 Hz	0.74 µA	7.4 V	60 mW/m^2	Sustainable Material Innovation, Green filler, Excellent Durability, Cost-effective approach.	This work

Abbreviations: TiO_2-Titanium dioxide; PCA-homogeneous PLA/CS/aloin, PNFM-porous nanofiber membrane, TPU-Thermoplastic polyurethanes, CB-Carbon black, CMCS-Carboxymethyl chitosan, CMC-Na carboxymethyl cellulose sodium, CANF- Cellulose acetate nanofiber, PEI- Polyethylenimine, GO- Graphene Oxide, CS-Chitosan.

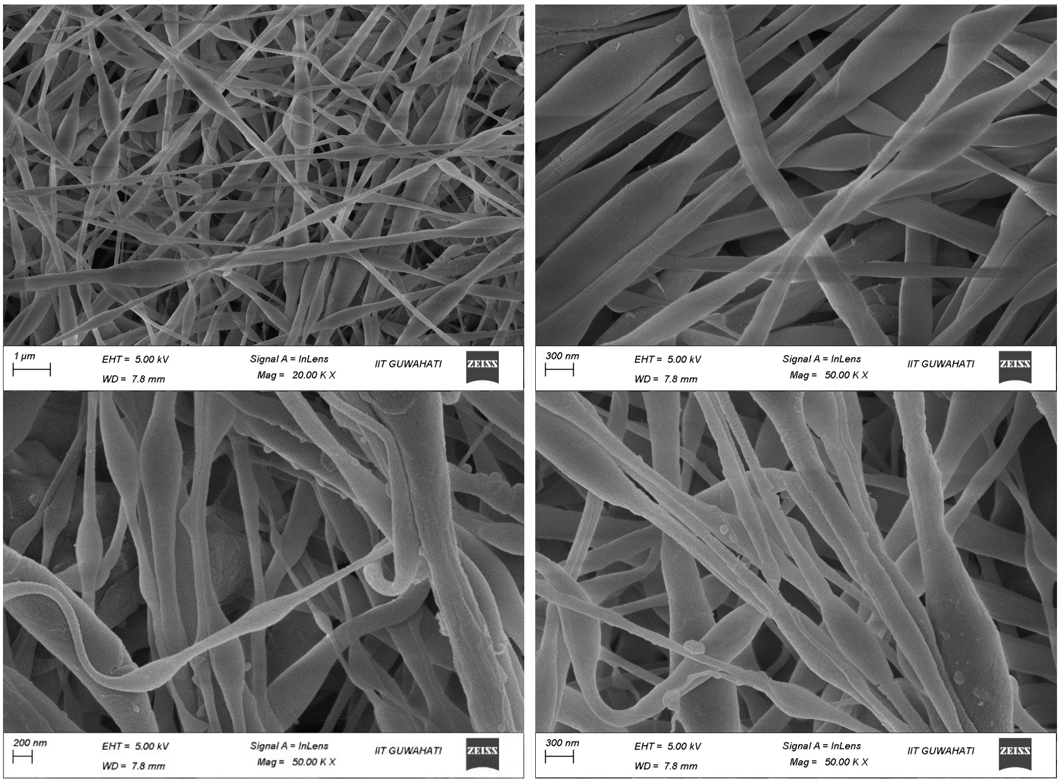

Fig .S9**.** FESEM images of P10-L5 at an initial stage

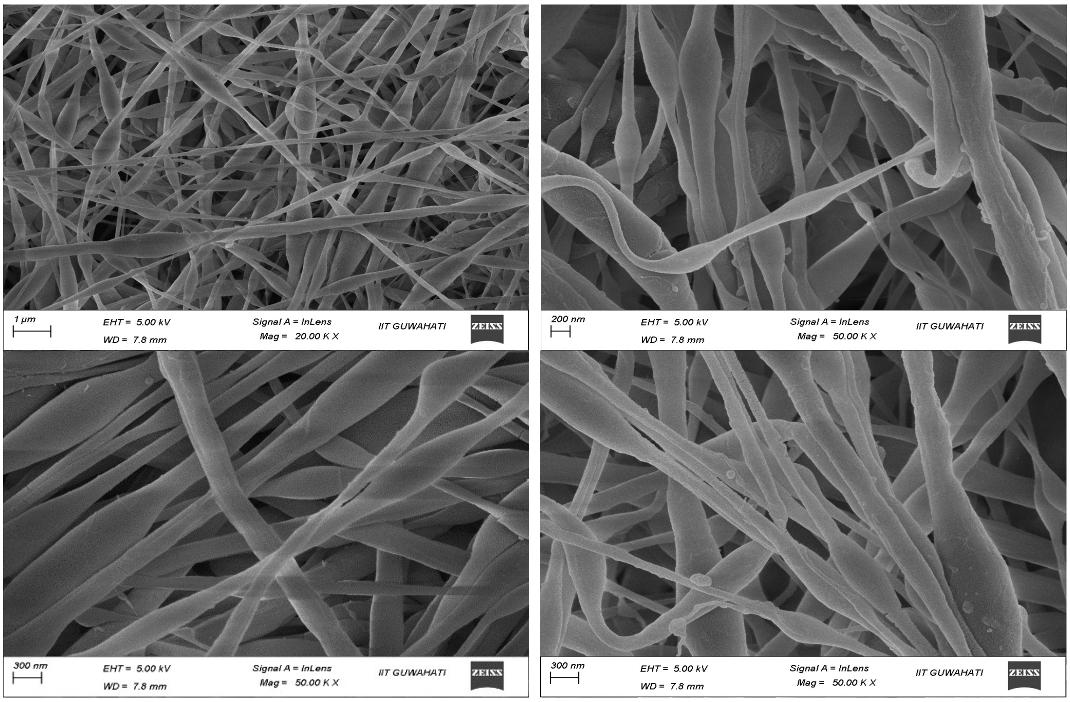

Fig .S10**.** FESEM images of P10-L5 after 10,000 working cycles.

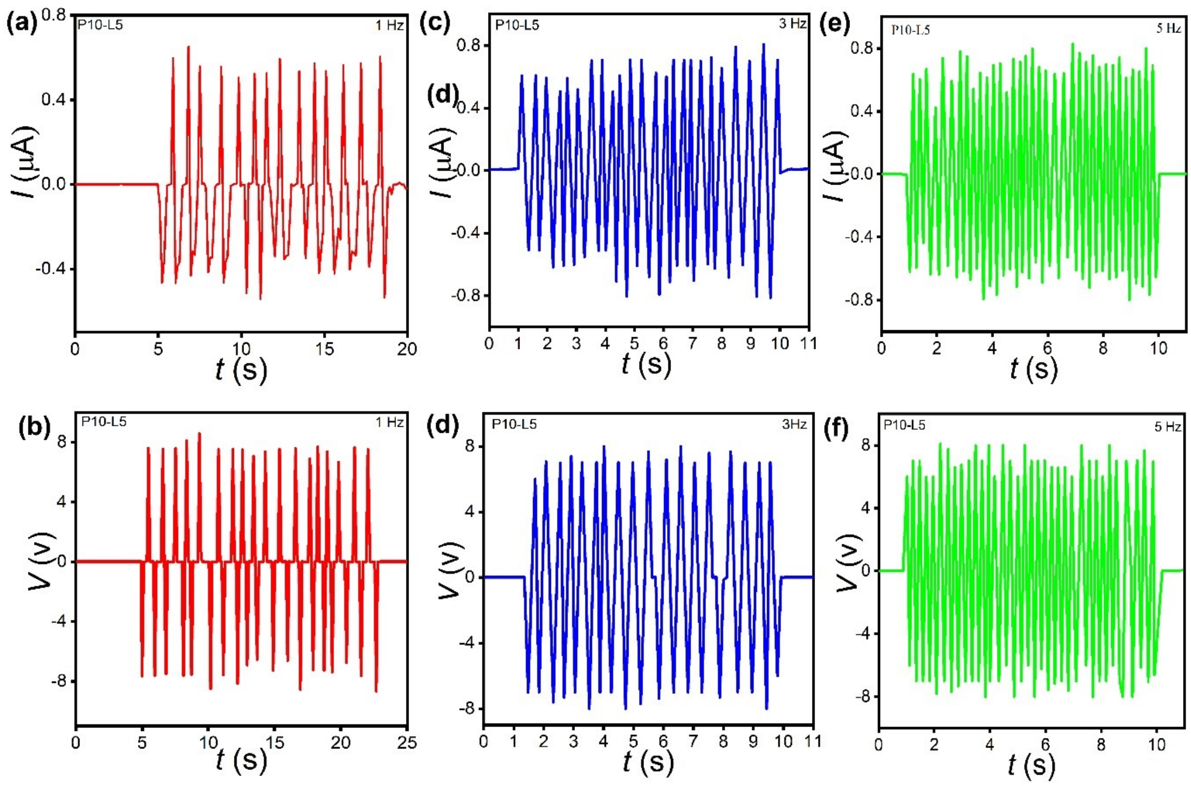

Fig. S11. output voltage and current of P10-L5 TENG at frequencies of 1Hz, 3Hz, and 5Hz.

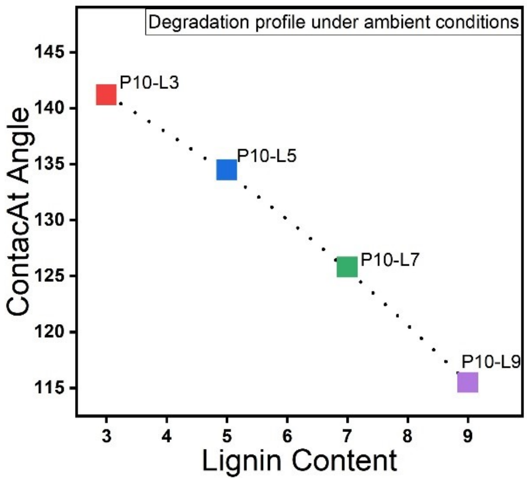

Fig. S12. Degradation sensitivity of nanofiber in ambient conditions.

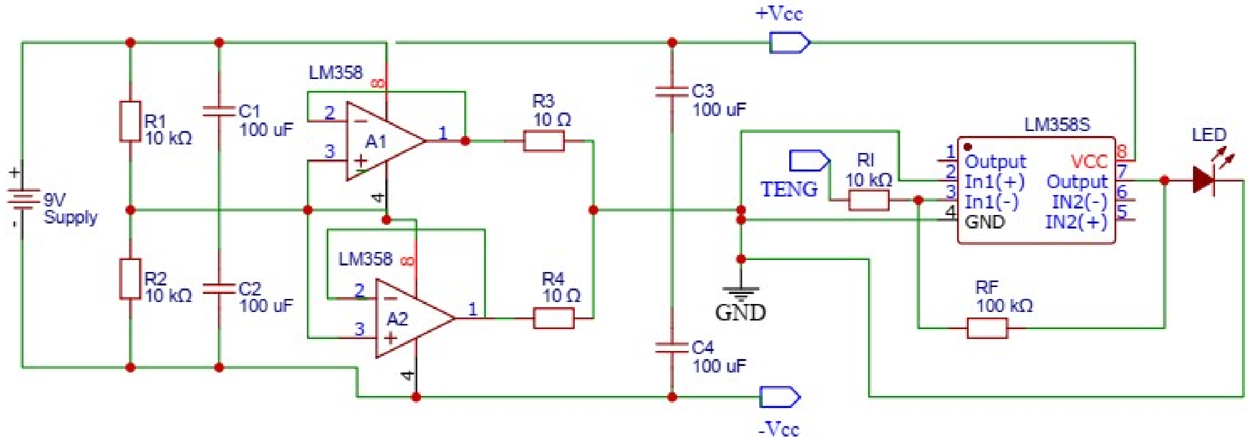

Fig. S13. Amplification circuit tailored for a TENG .

(1) Sluiter, A.; Hames, B.; Ruiz, R.; Scarlata, C.; Sluiter, J.; Templeton, D.; Crocker, D. *Determination of Structural Carbohydrates and Lignin in Biomass: Laboratory Analytical Procedure (LAP) (Revised July 2011)*; 2008. http://www.nrel.gov/biomass/analytical_procedures.html.

(2) Thomas-Kochakkadan, S.; Duque, M.; Murillo, G.; Nirwan, V. P.; Fahmi, A. Sustainable Electrospun Hybrid Nanofibers for Triboelectric Nanogenerators. *Small* **2025**, *21* (9). https://doi.org/10.1002/smll.202410271.

(3) Kim, J. N.; Lee, J.; Go, T. W.; Rajabi-Abhari, A.; Mahato, M.; Park, J. Y.; Lee, H.; Oh, I. K. Skin-Attachable and Biofriendly Chitosan-Diatom Triboelectric Nanogenerator. *Nano Energy* **2020**, *75*. https://doi.org/10.1016/j.nanoen.2020.104904.

(4) Yin, J.; Wang, J.; Ramakrishna, S.; Xu, L. All-Electrospun Triboelectric Nanogenerator Incorporating Carbon-Black-Loaded Nanofiber Membranes for Self-Powered Wearable Sensors. *ACS Appl Nano Mater* **2023**, *6* (17), 15416–15425. https://doi.org/10.1021/acsanm.3c01891.

(5) Qiu, Y.; Fang, H.; Guo, J.; Wu, H. Fully Nano/Micro-Fibrous Triboelectric on-Skin Patch with High Breathability and Hydrophobicity for Physiological Status Monitoring. *Nano Energy* **2022**, *98*. https://doi.org/10.1016/j.nanoen.2022.107311.

(6) Yan, K.; Li, X.; Wang, X. X.; Yu, M.; Fan, Z.; Ramakrishna, S.; Hu, H.; Long, Y. Z.; Wang, X. X.; Long, Y. Z. A Non-Toxic Triboelectric Nanogenerator for Baby Care Applications. *J Mater Chem A Mater* **2020**, *8* (43), 22745–22753. https://doi.org/10.1039/d0ta08909e.

(7) Varghese, H.; Abdul Hakkeem, H. M.; Farman, M.; Thouti, E.; Pillai, S.; Chandran, A. Self-Powered Flexible Triboelectric Touch Sensor Based on Micro-Pyramidal PDMS Films and

Cellulose Acetate Nanofibers. *Results in Engineering* **2022**, *16*. https://doi.org/10.1016/j.rineng.2022.100550.

(8) Shyju, S.; Chandran, A. M.; Varun, S.; Kumar, M. V. P.; Mural, P. K. S. Chitosan Nanocomposite-Based Triboelectric Nanogenerators with Enhanced Electrical Performance: An Opportunity for Bioelectronics. *ACS Appl Electron Mater* **2024**, *6* (2), 887–900. https://doi.org/10.1021/acsaelm.3c01428.